

High- T_c superconductivity in $\text{La}_3\text{Ni}_2\text{O}_7$ based on the bilayer two-orbital t - J model

Zhihui Luo,^{1,*} Biao Lv,^{1,*} Meng Wang,¹ Wéi Wú,^{1,†} and Dao-Xin Yao^{1,‡}

¹Center for Neutron Science and Technology, Guangdong Provincial Key Laboratory of Magnetoelectric Physics and Devices, State Key Laboratory of Optoelectronic Materials and Technologies, School of Physics, Sun Yat-Sen University, Guangzhou, 510275, China

(Dated: August 16, 2024)

The recently discovered high- T_c superconductor $\text{La}_3\text{Ni}_2\text{O}_7$ has sparked renewed interest in the unconventional superconductivity. Here we study superconductivity in pressurized $\text{La}_3\text{Ni}_2\text{O}_7$ based on a bilayer two-orbital $t - J$ model, using the renormalized mean-field theory. Our results reveal a robust s^\pm -wave pairing driven by the inter-layer d_{z^2} magnetic coupling, which exhibits a transition temperature within the same order of magnitude as the experimentally observed $T_c \sim 80$ K. We establish a comprehensive superconducting phase diagram in the doping plane. Notably, the $\text{La}_3\text{Ni}_2\text{O}_7$ under pressure is found situated roughly in the optimal doping regime of the phase diagram. When the $d_{x^2-y^2}$ orbital becomes close to half-filling, d -wave and $d + is$ pairing can emerge from the system. We discuss the interplay between Fermi surface topology and different pairing symmetries. The stability of the s^\pm -wave pairing against Hund's coupling and other magnetic exchange couplings is discussed.

Keywords: superconductivity, bilayer nickelate, transition temperature, pairing symmetry, t - J model.

I. INTRODUCTION

Understanding high transition temperature (T_c) superconductivity remains one of the greatest challenges in the condensed matter physics. For cuprate superconductors [1–3], the fundamental mechanism of the d -wave pairing is believed to primarily lie in the $d_{x^2-y^2}$ orbital, with strong Coulomb repulsion between electrons playing a crucial role[2]. This form of superconductivity is usually referred to as unconventional, distinguishing it from the traditional Bardeen-Cooper-Schrieffer (BCS) type of superconductivity. Another prominent example of the unconventional superconductivity is found in the iron-based superconductors [4–8], where multiple d -orbitals participate in the pairing process. The discovery of superconductivity in infinite-layer $\text{Nd}_{1-x}\text{Sr}_x\text{NiO}_2$ thin films has sparked widespread interest due to cuprate-like $\text{Ni}^{1+}(3d^9)$ [9–16]. Most recently, a Ruddlesden-Popper nickelate superconductor $\text{La}_3\text{Ni}_2\text{O}_7$ is found with a $T_c \approx 80$ K [17–19] under moderate pressures. On one hand, $\text{La}_3\text{Ni}_2\text{O}_7$ shares similarities with cuprates, as both feature the $\text{NiO}_2/\text{CuO}_2$ plane containing a key $d_{x^2-y^2}$ orbital at Fermi level. On the other hand, $\text{La}_3\text{Ni}_2\text{O}_7$ differs from cuprates as its apical $\text{O}-p_z$ and $\text{Ni}-d_{z^2}$ orbitals play a significant role in its low-energy physics [17, 20]. Given this context, one would ask that whether the underlying pairing mechanism of $\text{La}_3\text{Ni}_2\text{O}_7$ resembles that of cuprates? How does it differ from the extensively studied cuprates? From a theoretical perspective, a first step in addressing these questions is to resolve the roles played by the $d_{x^2-y^2}$ and d_{z^2} orbitals in pairing, and to con-

struct a superconducting phase diagram of the relevant physical models.

Electronic structure studies [21–27] and optical experimental probe [28] suggest that in pressurized $\text{La}_3\text{Ni}_2\text{O}_7$, $\text{Ni}-d_{z^2}$ orbital is involved in Fermi energy due to strong inter-layer coupling via apical oxygen. Through hybridization with the in-plane oxygen p -orbital, d_{z^2} orbitals can mix with $d_{x^2-y^2}$ orbitals, resulting in a three-pocket Fermi surface structure[21]. This Fermi surface geometry differs from that of cuprates, which may lead to pairing symmetry and effective pairing “glue” distinct from that of the d -wave superconductivity in cuprates, which arises upon doping a single $d_{x^2-y^2}$ orbital. Another crucial consideration is the electron occupancy. $\text{La}_3\text{Ni}_2\text{O}_7$ typically exhibits a nominal valence configuration of $d^{7.5}$ [17, 29], indicating an average of 2.5 holes in the active e_g sub-shell. While previous studies have shown variations in the computed electron densities of the two e_g orbitals[30–34], it can be in general viewed as a multi-orbital system comprising a heavily hole-doped $d_{x^2-y^2}$ orbital (with a hole density ~ 1.5), and a near half-filled d_{z^2} orbital (with a hole density ~ 1.0). Regarding superexchange couplings, investigation based on cluster dynamical mean-field theory [30] have pointed out that the exchange coupling between two inter-layer d_{z^2} orbitals J_\perp may be substantially larger, by a factor of at least ~ 2 , than the intra-layer $d_{x^2-y^2}$ exchange coupling J_\parallel , with the latter estimated to be comparable to its cuprate counterpart [30]. Such a significant J_\perp is likely responsible for the high transition T_c in $\text{La}_3\text{Ni}_2\text{O}_7$ [30, 31, 35–39].

In this paper, we systematically investigate superconductivity in the bilayer two orbital $t - J$ model, which serves as a prototype for the low-energy physics of pressurized $\text{La}_3\text{Ni}_2\text{O}_7$, using the renormalized mean-field theory (RMFT) [40–42]. The RMFT approach is a con-

* These authors contributed equally to this work

† wuwei69@mail.sysu.edu.cn

‡ yaodaoy@mail.sysu.edu.cn

crete implementation of Anderson’s resonating valence bond (RVB) concept of the unconventional superconductivity [43]. Following the Gutzwiller scheme, the renormalization effects from strong electron correlations are accounted on different levels by incorporating the doping-dependent renormalization factors g_t, g_J [40] in RMFT. The mean-field decomposition of the magnetic exchange couplings J , then enables exploring of the BCS pairing instabilities within the system. Despite its straightforward formulations, RMFT has demonstrated its capability of capturing various aspects of cuprate superconductors, including superfluid density, the dome-shaped doping dependence of T_c , and pseudogap phenomena [41]. In RMFT, the superconducting order parameter $g_t\Delta$ involves two competing energy scales: the phase coherence energy scale associated with g_t , and the pairing amplitude represented by Δ , each exhibiting distinct doping dependencies [40]. In our study, we observe that the outcome of this competition positions $\text{La}_3\text{Ni}_2\text{O}_7$ within the optimal doping regime in the superconducting phase diagram. Our calculation suggests a T_c comparable to experimental observations, indicating the relevance of our considerations to the $\text{La}_3\text{Ni}_2\text{O}_7$ superconductor. Furthermore, we elucidate various possible pairing symmetries across a broad doping range.

The remainder of paper is organized as follows. In Sec. IV, we present the physical model and describe the RMFT method. In Sec. II, we present our results including T_c for the pristine compound, the doping phase diagram, and the Fermi surface. Additionally, the impact of the strength of superexchanges and Hund’s coupling is discussed at the end of the section. In Sec. III we discuss the stability of the s^\pm -pairing. Finally, more details can be found in the Supplementary Information.

II. RESULTS

Now we present the RMFT result on the superconducting instabilities of the bilayer two-orbital $t-J$ model. In particular, we provide detailed investigations in the parameter regime that most relevant to the $\text{La}_3\text{Ni}_2\text{O}_7$ system. The impacts of several key factors including temperature T , doping levels of $d_{x^2-y^2}$, and d_{z^2} orbitals: p_x, p_z , as well as the geometry of Fermi surface are analyzed while eyeing on the evolution of the superconducting order parameter $g_t^{\alpha\beta}|\Delta_\ell^{\alpha\beta}|$. The definition of $g_t^{\alpha\beta}|\Delta_\ell^{\alpha\beta}|$ and RMFT formalism can be found in Methods. For brevity, we adopt the shorthand notation $g_t^\nu|\Delta_\ell^\nu|$ in the following discussion to represent $g_t^{\alpha\beta}|\Delta_\ell^{\alpha\beta}|$, where $\ell = d, s^\pm$, denoting pairing symmetries, and $\nu = ||x, ||z, \perp z$ denoting intra-layer $d_{x^2-y^2}$ $[(\alpha, \beta) = (x_1, x_1)]$, intra-layer d_{z^2} $[(\alpha, \beta) = (z_1, z_1)]$ and inter-layer d_{z^2} $[(\alpha, \beta) = (z_1, z_2)]$ pairing. Without loss of generality, we adopt typical values of $J_\perp = 2J_\parallel = 0.18$ eV taken from Ref. [30] throughout the paper unless otherwise specified.

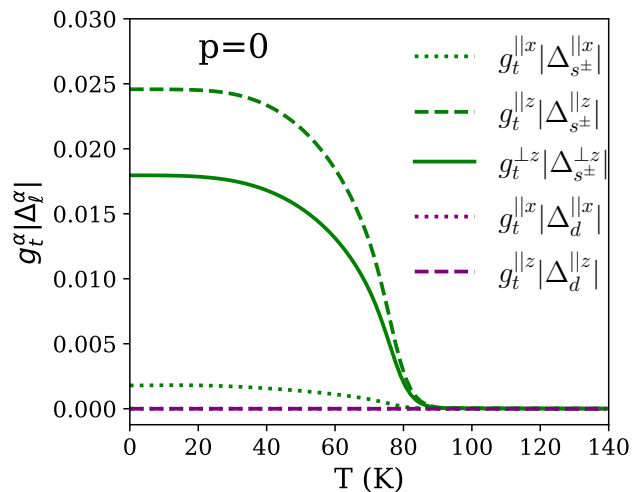


FIG. 1. Superconducting order parameters $g_t^\nu|\Delta_\ell^\nu|$ as a function of temperature T . Note that the two purple lines overlap with each other with zero magnitude over the whole temperature range. Since here the doping is fixed as $p = 0$ ($n_x = 0.665, n_z = 0.835$), g_t^ν is constant according to Eq. (5-6).

A. T_c for pristine compound

We first present the RMFT calculated superconducting transition temperature T_c at $\mu = 0$ that corresponds to pristine $\text{La}_3\text{Ni}_2\text{O}_7$ under pressure, which is to be dubbed as the pristine compound (PC) case hereafter. For the PC case, we have $\mu = 0, n_x = 0.665, n_z = 0.835$, and $n = n_x + n_z = 1.5$ [21]. In Fig. 1, the superconducting order parameter $g_t^\nu|\Delta_\ell^\nu|$ is plotted as a function of T , which clearly demonstrate two dominant branches of the pairing fields at small T : the intra-layer d_{z^2} pairing (dashed line) and the inter-layer d_{z^2} pairing (solid line), forming the s^\pm -wave pairing of the system. This result is in agreement with several other theoretical studies [36, 38, 39, 44–46]. As increasing T , the order parameters decrease in a mean-field manner and eventually drop to zero at around 80 K. The computed value of T_c is somehow coincides with the experiment [17], highlighting that the various energy scales under our consideration can effectively capture the major physics of the realistic compound. However, we would like to stress that the superconducting T_c from RMFT in fact dependent on the value of J essentially in a BCS manner. Hence it can be sensitive to the strength of the superexchange couplings. The coincidence between the experimental and RMFT value of T_c should not be taken as the outcome of RMFT capturing $\text{La}_3\text{Ni}_2\text{O}_7$ superconductivity in a quantitatively correct way. We note that the s^\pm -wave pairing has also finite $d_{x^2-y^2}$ orbital component, as shown by the dotted lines in Fig. 1, despite that its order parameter are much smaller than that of the d_{z^2} orbitals. The d -wave order parameters (purple), on the other hand, are fully suppressed, suggesting that the $d + is$ -wave pairing in-

stability may be ruled out in our model for $\text{La}_3\text{Ni}_2\text{O}_7$. It is worthy noting that RMFT is originally formulated at zero temperature [40]. In Fig. 1 we solve the RMFT equations in the finite temperature regime [47]. This extension captures finite temperature effects on the mean-field parameters Δ and χ , while neglecting thermal effects on the renormalization factors g_t, G_{J_r} . We argue that the latter should have insignificant impacts on determining T_c , given the hole concentrations in Fig. 1, ($n_x^h = 1 - n_x \approx 0.335, n_z^h = 1 - n_z \approx 0.165$) are fairly large. Detailed discussions on this matter can be found in the Supplementary Note 2.

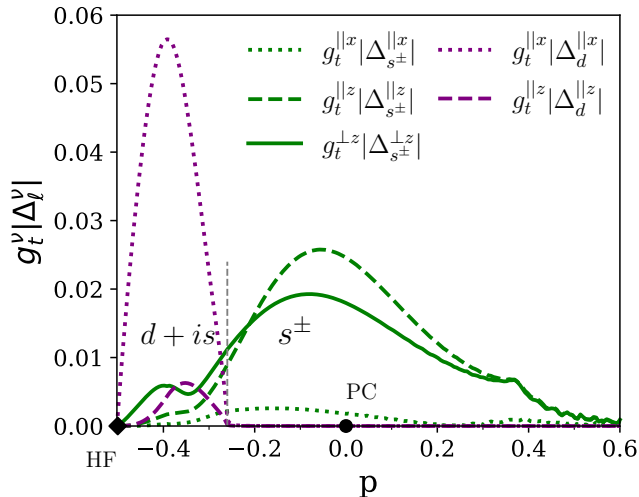


FIG. 2. Superconducting order parameter $g_t^\nu |\Delta_\ell^\nu|$ as a function of doping p . $p > 0$ represents hole doping the pristine compound case (where $n_x = 0.665, n_z = 0.835$), and $p < 0$ for electron doping. Black dot at $p = 0$ indicates the pristine compound (PC). We vary p while a fixed ratio of $p_x/p_z = 2.048$ is maintained. The two e_g orbitals reach half-filling (HF) ($n_x = 1.0, n_z = 1.0$) at $p = -0.5$, as indicated by the diamond symbol.

B. Doping evolution

Now we focus on the doping dependence of the superconducting order parameter $g_t^\nu |\Delta_\ell^\nu|$. In the following, $p > 0$ means doping the pristine compound (where $n_x = 0.665, n_z = 0.835$) with holes, and $p < 0$ denotes electron doping. While varying the doping level p of the system, we maintain a fixed ratio between the doping levels of the two e_g orbitals, namely, $p_x/p_z = 2.048$ is fixed, such that both e_g orbitals are half-filling (HF), *i.e.*, $n_x = 1, n_z = 1$ at $p = -0.5$. From Fig. 2, one learns that the s^\pm -wave pairings (green) are quite robust over a wide range of doping p . The maxima of $g_t^\nu |\Delta_{s^\pm}^\nu|$ are located at $p \approx -0.04$ which is very close to $p = 0$ for PC. This indicates that, interestingly, the $\text{La}_3\text{Ni}_2\text{O}_7$ under pressure corresponds to roughly the optimal doping in our superconducting phase diagram. At extremely large

electron dopings ($p < -0.25$), d -wave pairing can build up which also exhibits a predominant superconducting dome (purple dotted line). In this doping regime, small s^\pm -wave components of the superconducting order parameter are found to coexist with the d -wave components, indicating the emergence of $d + is$ -wave pairing. At half-filling in Fig. 2 ($p = -0.5$), all pairing channels are fully suppressed due to the vanishing renormalization factors $g_t^\nu \rightarrow 0$, reflecting the Mott insulating nature at half-filling [30].

It is worth noting that, as a general prescription of the mean-field approaches, different J_r terms in Eq. 4 can be decomposed into different corresponding pairing bonds Δ_δ , such as $\Delta_{d/s^\pm}^{\perp z}$ from decomposing J_\perp , and $\Delta_{d/s^\pm}^{\parallel x}$ from decomposing J_\parallel . Note that in our calculation, the pairing components $\Delta_{d/s^\pm}^{\parallel z}$ (dashed lines in Fig. 2) that represent the intra-layer pairing of d_{z^2} orbital, do not have a corresponding J term in the Hamiltonian. Their values are not determined by the competition between $\Delta_{d/s^\pm}^{\parallel z}$ and $|\Delta_{d/s^\pm}^{\parallel z}|^2$ terms in minimizing the free-energy. Instead, it should be interpreted as the pairing instability induced by the pre-existing inter-layer d_{z^2} pairing. Indeed, as shown in Fig. 2, $\Delta_{s^\pm}^{\parallel z}$ displays a doping p -dependence similar to that of $\Delta_{s^\pm}^{\perp z}$. Finally, we notice that a small tip appears at hole doping $p \sim 0.4$, which can be attributed to the van Hove singularity associated with the β -sheet of the Fermi surface, see also Section IID.

C. Doping phase diagram

To gain further insights into the RMFT result of $\text{La}_3\text{Ni}_2\text{O}_7$ system, we obtain a phase diagram in the $p_x - p_z$ doping plane where now the two dopings are independent variables. As shown in Fig. 3, RMFT reveals that d , s^\pm , and $d + is$ pairing symmetries, as well as the normal state occur in different doping regimes. Here a dashed white line indicates the $p_x - p_z$ trajectory along which Fig. 2 is plotted. The black symbols label out sets of (p_x, p_z) parameters on which the result will be further discussed in Fig. 5. The major feature of Fig. 3 is that the d -wave and s^\pm -wave pairings span roughly a vertical and a horizontal stripe respectively in the phase diagram. In other words, s^\pm -wave pairing (green) dominates the regime where $-0.1 \lesssim p_z \lesssim 0.1$ ($0.735 \lesssim n_z \lesssim 0.935$), and it is insensitive to the value of p_x . Likewise, the d -wave pairing (purple) prevails in the doping range of $-0.335 \lesssim p_x \lesssim -0.2$ ($0.465 \lesssim n_x \lesssim 1.0$), and it is in general less sensitive to the value of p_z . As a result, the $d + is$ -wave pairing (orange) naturally emerges at the place where the two stripes overlap. In order to have a better understanding of this phase diagram, we show the magnitudes of the four major pairing bond $g_t^\nu |\Delta_\ell^\nu|$ in Fig. 4, from which one sees that for s^\pm -wave pairing, the pairing tendencies of $\Delta_{s^\pm}^{\perp z}$ (Fig. 4a)

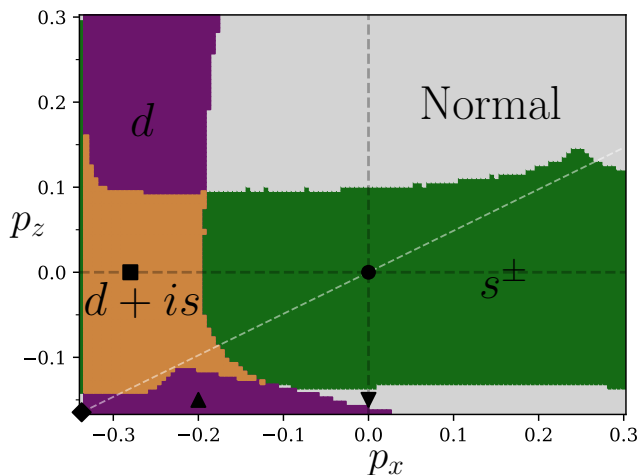


FIG. 3. Pairing phase diagram constructed by varying doping levels p_x and p_z . $p_x > 0$ indicates hole doping and $p_x < 0$ denotes electron doping relative to the pristine compound case ($n_x = 0.665, n_z = 0.835$). The dashed white line presents the $p_x - p_z$ trajectory along which Fig. 2 is plotted. The black symbols mark the sets of (p_x, p_z) that are further discussed in Fig. 5. The superexchange couplings applied are $J_\perp = 2J_\parallel = 0.18$.

and $\Delta_{s^\pm}^{\parallel z}$ (Fig. 4b) show similar pattern in the $p_x - p_z$ plane, in consistence with Fig. 2. For the d -wave pairing, the situation is however different. For intra-layer pairing, $g_t^{\parallel x} |\Delta_d^{\parallel x}|$ is enhanced when $d_{x^2-y^2}$ is heavily electron doped ($p_x \approx -0.25$), and d_{z^2} becomes half-filling ($p_z \sim -0.2$). This is because the large electron doping drives the γ -pocket of d_{z^2} orbital centered at M -point descends into the Fermi sea. Such that the system becomes effectively a single band system of the active $d_{x^2-y^2}$ orbital. Hence the dominant d -wave pairing of the single-band $t - J$ model is recovered for $d_{x^2-y^2}$ orbital in this limit, mimicking the physics of cuprates. On the other hand, the d_{z^2} component of the d -wave pairing $g_t^{\parallel z} |\Delta_d^{\parallel z}|$ is enhanced when $p_z > 0.2$, as shown in Fig. 4d. This can be understood considering the fact that since intra-layer exchange of d_{z^2} orbital $J_{\parallel z} = 0$ in our study, the d -wave instability driven by J_{\parallel} of the $d_{x^2-y^2}$ orbital is less sensitive to the details of d_{z^2} orbital. Hence, the order parameter $g_t^{\parallel z} |\Delta_d^{\parallel z}|$ increasing with p_z shown in Fig. 4d can be seen vastly as a result of a growing $g_t^{\parallel z}$ with decreasing n_z according to Eq. (5-6). Finally, it is interesting to note that although $J_\perp = 2J_\parallel$ is used in our study, Fig. 4 shows that the the maximal value of d -wave superconducting order parameter are roughly two times larger than that of the s^\pm -wave pairing. This is expected since the vertical exchange coupling J_\perp has a smaller coordination number $z = 1$, compared to its the in-plane counterpart J_\parallel , where $z = 4$.

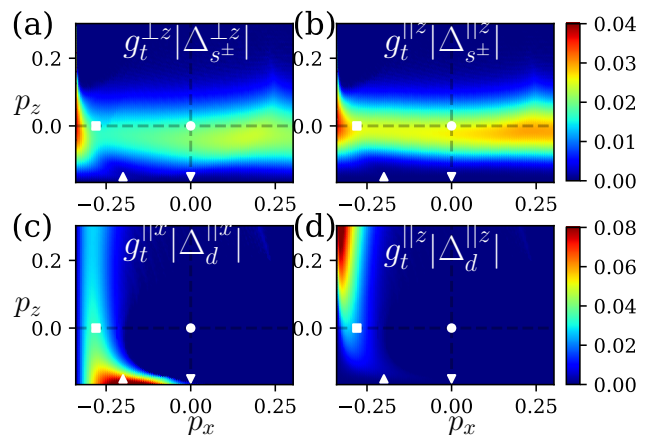


FIG. 4. Superconducting order parameters $g_t^\nu |\Delta_\ell^\nu|$ with varying doping levels p_x and p_z . Again, here $(p_x = 0, p_z = 0)$ corresponds to $(n_x = 0.665, n_z = 0.835)$. Symbols denote typical dopings to be analyzed in Fig. 5.

D. Fermi surfaces

In Fig. 5 we display the paring gap function Δ_ℓ^ν projected onto the Fermi surfaces for four typical sets of dopings (p_x, p_z) with each characterizing one type of pairing symmetries (Fig. 5a, Fig. 5b, Fig. 5d) or the one with vanishing superconducting order parameter (Fig. 5c). Fig. 5a shows the FS of the PC case with s^\pm pairing, which has three sheets of FS with one around Γ point and two around M point [21]. Also, the sign structure is consistent with that in Refs. [36, 39, 45]. The key feature here is that the sign of the pairing gap is the same within the α, γ bands, but it reverses between α/γ and β pockets. This is because the former two components come from the bonding state while the latter is from the anti-bonding state. Decreasing p_x from the PC can drives the $d_{x^2-y^2}$ orbital closer to half-filling. As shown in Fig. 5b, the α, β -sheet of FS as a whole is also driven closer to the folded Brillouin zone (FBZ) edge (dashed lines), which is accompanied by the the pairing symmetry evolving from s^\pm to $d + is$ -wave. In this case, we see that the α, β pockets exhibit the d -wave sign structure while the γ pocket maintains the s -wave symmetry, and, its profile is less affected by the changing of p_x . The occurrence of the d -wave pairing at this doping level unambiguously signals the importance of the intra-orbital physics in $d_{x^2-y^2}$ orbital as it approaches half-filling. Fig. 5c displays that as lowering p_z from the PC case, the γ -pocket vanishes from the Brillouin zone. Consequently, the s^\pm -wave order parameter vanishes at $p_z \sim -0.15$. In this case, similar to PC, no finite d -wave order parameter is observed. Note that the gap magnitude in Fig. 5 is associated with Δ_ℓ^ν instead of the superconducting order parameter $g_t^\nu |\Delta_\ell^\nu|$, which is why Fig. 5c shows nonvanishing gap for a normal state, see also Supplementary Note 4. Fig. 5d shows the last case with the γ -pocket

vanishing from Fermi level. As expected, in this case, only the d -wave pairing with finite $g_t^{\parallel x} |\Delta_d^{\parallel x}|$ is found. As discussed above, here the physics of the system can be essentially captured by the single-band $t - J$ model with the presence of only $d_{x^2-y^2}$ orbital.

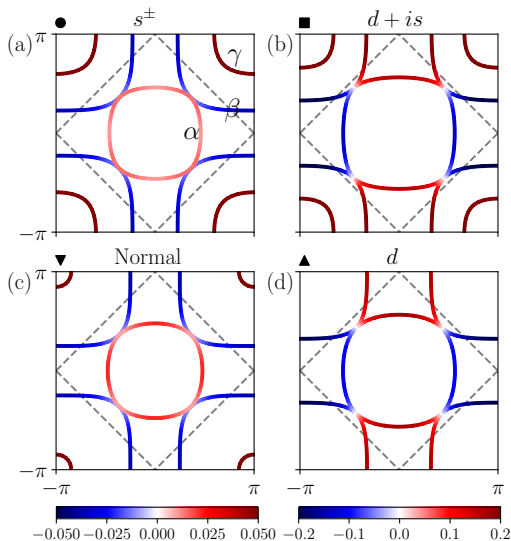


FIG. 5. The pairing gap function Δ_ℓ^ν projected onto the Fermi surface for a few sets of (p_x, p_z) . Dot: $(p_x = 0, p_z = 0)$, square: $(p_x = -0.28, p_z = 0)$, upper triangle: $(p_x = -0.2, p_z = -0.15)$, and lower triangle: $(p_x = 0, p_z = -0.15)$. See also symbols indicated in Fig. 3 and 4. Note that the gap magnitudes are directly associated with Δ_ℓ^ν instead of the superconducting order parameter $g_t^\nu |\Delta_\ell^\nu|$, which is why (c) shows nonvanishing gap for a normal state. The dashed lines indicate the folded Brillouin zone (FBZ) of the two in-plane Ni.

E. Superexchanges J

Finally, we investigate the influence of the magnitudes of the superexchanges for the pristine compound. In Fig. 6, we present $g_t^\nu |\Delta_\ell^\nu|$ as a function of J_{\parallel}/J_{\perp} . A vertical arrow indicates the value of J_{\parallel}/J_{\perp} used in aforementioned calculations, where s^{\pm} -wave is found for PC. As decreasing/increasing J_{\parallel}/J_{\perp} , s^{\pm} -wave order parameters (green lines) decrease/increase very slightly with J_{\parallel}/J_{\perp} . When $J_{\parallel}/J_{\perp} \sim 1.1$, d -wave (purple solid line) starts to build up at $d_{x^2-y^2}$ orbital. For $\text{La}_3\text{Ni}_2\text{O}_7$ under pressure, this large value of J_{\parallel}/J_{\perp} is however not very realistic [30]. Hence, the d -wave pairing instability may be excluded for the realistic materials in our study. To check the stability of the superconductivities, results for $J_{xz} = 0.03$ (dashed line) and $J_H = -1$ eV (dash-dotted line) are shown in Fig. 6. As one sees that, although both J_{xz} and J_H act as pair-breaking factors, they do not significantly modify the result we obtained above. In particular, for the s^{\pm} -pairing, the changes of

the order parameter $g_t^\nu |\Delta_\ell^\nu|$ caused by J_{xz} (green dashed line) and J_H (not shown here) are negligible.

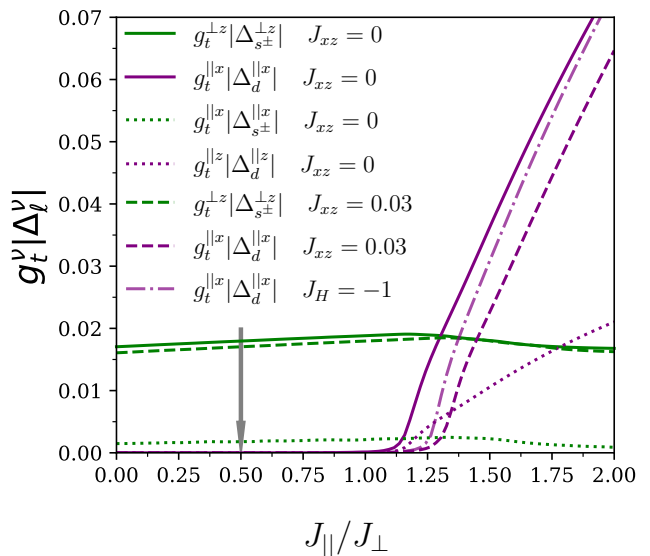


FIG. 6. Superconducting order parameters $g_t^\nu |\Delta_\ell^\nu|$ as a function of J_{\parallel}/J_{\perp} for the pristine compound. The solid and dotted lines denote cases of $J_{xz} = 0$, dashed lines denote that of $J_{xz} = 0.03$ eV, and dash-dotted line denotes the case of $J_H = -1$ eV. Here $J_{\perp} = 0.18$ eV is fixed. The vertical arrow indicates $J_{\parallel}/J_{\perp} = 0.5$ which is used in our above calculations.

III. DISCUSSION

In our study, the RMFT equations are solved in such a way that the pairing fields on different bonds are varied independently, namely, no specific pairing symmetry is presumed in the self-consistent process. The symmetries of the electron pairing naturally emerge as a result of energy minimization in our calculations, preventing the potential overlooking of pairing symmetries. Regarding the dominant s^{\pm} pairing for the pristine compound at $p_x, p_z = 0$, we note that even when only J_{\perp} is considered (with $J_{\parallel} = 0, J_{xz} = 0$), $\Delta^{\parallel x}$ is finite although much smaller than $\Delta^{\parallel z}$ and $\Delta^{\perp z}$. Given the smaller effective mass of the $d_{x^2-y^2}$ orbital compared to the d_{z^2} orbital, it may still contribute significantly to the superfluid density in the superconducting state of the system. The dual effects of the Hund's coupling J_H , namely, the alignment of the on-site spins of the $d_{x^2-y^2}$ and d_{z^2} orbitals, and the enhancement of J_{\parallel} and J_{xz} couplings, show no significant impact on the dominant s^{\pm} pairing in our RMFT study, as indicated in Fig. 6. However, we acknowledge that the implications of J_H on superconductivity may be underestimated in the RMFT formalism [48]. Additionally, it is important to note that the superconducting T_c obtained by RMFT is generally overestimated because both temporal and spatial fluctuations are neglected. This is par-

ticular true when considering that the pairing fields originate from the local inter-layer d_{z^2} magnetic couplings, where phase fluctuations can play a more significant role in suppressing T_c comparing to its single-band $t-J$ model counterpart in cuprate superconductors. Finally, a recent theory work [31] proposes that within the framework of the two-component pairing theory in a composite system, the phase fluctuations can be suppressed by the hybridization effects between $d_{x^2-y^2}$ and d_{z^2} orbitals. Verifying this conjecture is, however, beyond the scope of this work.

Employing the renormalized mean-field theory, we have established a comprehensive superconducting phase diagram for the bilayer two-orbital $t-J$ model. A robust s^\pm -wave pairing is found to exist in the parameter regime relevant to $\text{La}_3\text{Ni}_2\text{O}_7$ under pressure, which in general corresponds to the optimal doping of the superconducting phase diagram. We have carefully investigated the dependence of the pairing instabilities on doping levels, exchange couplings, and the effects of Hund's coupling. Our study provides significant insights into the theoretical understanding of the superconductivity $\text{La}_3\text{Ni}_2\text{O}_7$ under pressure.

IV. METHODS

A. Model

In the strong-coupling limit, the bilayer two orbital Hubbard model [21] can be mapped into a $t-J$ model [30]

$$\begin{aligned} \mathcal{H} &= \mathcal{H}_t + \mathcal{H}_J \quad (1) \\ \mathcal{H}_t &= \sum_{ij\alpha\beta\sigma} (t_{ij}^{\alpha\beta} - \mu\delta_{ij}\delta_{\alpha\beta})c_{i\alpha\sigma}^\dagger c_{j\beta\sigma} \\ &\quad + \epsilon_{xz} \sum_{i\sigma}^{\alpha\beta=x_1z_1, x_2z_2} (n_{i\alpha\sigma} - n_{i\beta\sigma}) \\ \mathcal{H}_J &= J_\perp \sum_i \mathbf{S}_{iz_1} \cdot \mathbf{S}_{iz_2} + J_{||} \sum_{\langle ij \rangle}^{\alpha=x_1, x_2} \mathbf{S}_{i\alpha} \cdot \mathbf{S}_{j\alpha} \\ &\quad + J_{xz} \sum_{\langle i, j \rangle}^{\alpha\beta=x_1z_1, x_2z_2} \mathbf{S}_{i\alpha} \cdot \mathbf{S}_{j\beta} + J_H \sum_i^{\alpha\beta=x_1z_1, x_2z_2} \mathbf{S}_{i\alpha} \cdot \mathbf{S}_{i\beta}, \end{aligned}$$

where \mathcal{H}_t is the tight-binding Hamiltonian taken from downfolding the DFT band structure [21], which is defined in a basis of $\Psi_{i\sigma} = (c_{ix_1\sigma}, c_{iz_1\sigma}, c_{ix_2\sigma}, c_{iz_2\sigma})^T$, with $c_{i\alpha\sigma}$ representing annihilation of an electron with spin σ on $\alpha = x_1, z_1, x_2, z_2$ orbital at i site. Here x_1, x_2 denote the two $\text{Ni-}3d_{x^2-y^2}$ orbitals situated in the double NiO_2 layer while z_1, z_2 correspondingly denote the two $\text{Ni-}3d_{z^2}$ orbitals. μ is the chemical potential and ϵ_{xz} is the energy difference between $d_{x^2-y^2}$ and d_{z^2} orbitals. The hopping parameters in \mathcal{H}_t used in this work can be found in Supplementary Note 1. \mathcal{H}_J is the Heisenberg exchange couplings, and the spin operator $\mathbf{S}_{i\alpha} = \frac{1}{2} \sum_{\mu\nu} c_{i\alpha\mu}^\dagger \boldsymbol{\sigma}_{\mu\nu} c_{i\alpha\nu}$.

According to the estimated antiferromagnetic correlations in $\text{La}_3\text{Ni}_2\text{O}_7$ [30], there can be three major magnetic exchange couplings $J_\perp, J_{||}, J_{xz}$, which respectively represents nearest-neighbor inter-layer exchange of d_{z^2} orbital, intra-layer exchange of $d_{x^2-y^2}$ and intra-layer exchange between $d_{x^2-y^2}$ and d_{z^2} . J_H is the intra-atomic Hund's coupling.

B. RMFT Formalism

To proceed with RMFT [40], we first define the following mean-field parameters

$$\chi_{ij}^{\alpha\beta} = \frac{1}{2} \langle c_{i\alpha\uparrow}^\dagger c_{j\beta\uparrow} + c_{i\alpha\downarrow}^\dagger c_{j\beta\downarrow} \rangle = \langle c_{i\alpha\uparrow}^\dagger c_{j\beta\uparrow} \rangle \quad (2)$$

$$\Delta_{ij}^{\alpha\beta} = \frac{1}{2} \langle c_{i\alpha\uparrow}^\dagger c_{j\beta\downarrow}^\dagger - c_{i\alpha\downarrow}^\dagger c_{j\beta\uparrow}^\dagger \rangle = \langle c_{i\alpha\uparrow}^\dagger c_{j\beta\downarrow}^\dagger \rangle, \quad (3)$$

where $\chi_{ij}^{\alpha\beta}$ and $\Delta_{ij}^{\alpha\beta}$ are particle-hole and particle-particle pairs relating $i\alpha$ and $j\beta$. Here we assume no magnetic ordering. For each type of exchange couplings J_r in Eq. (1), including the Hund's coupling J_H , the mean-field decomposition of \mathcal{H}_J introduces condensations of χ and Δ in the corresponding r -channel

$$H_{J_r}^\chi = -\frac{3}{4} J_r \sum_{\langle ij \rangle > \sigma} (\chi_\delta^{\alpha\beta} c_{i\alpha\sigma}^\dagger c_{j\beta\sigma} + h.c.) + \frac{3}{2} J_r N |\chi_\delta^{\alpha\beta}|^2, \quad (4)$$

$$H_{J_r}^\Delta = -\frac{3}{4} J_r \sum_{\langle ij \rangle > \sigma} (\sigma \Delta_\delta^{\alpha\beta} c_{i\alpha\sigma}^\dagger c_{j\beta\bar{\sigma}}^\dagger + h.c.) + \frac{3}{2} J_r N |\Delta_\delta^{\alpha\beta}|^2.$$

Assuming translation symmetry, $\delta = R_{j\beta} - R_{i\alpha}$ denotes different bonds in real-space associated with J_r , and N is the total number of sites of the square lattice.

We now introduce two renormalization factors [49]

$$G_t^\alpha = \sqrt{\frac{1 - n_\alpha}{1 - n_\alpha/2}}, \quad G_J^\alpha = \frac{1}{(1 - n_\alpha/2)}. \quad (5)$$

These two quantities essentially reflect the renormalization effects by the electrons repulsions on top of the single-particle Hamiltonian in the Gutzwiller approximation [40, 42, 50, 51], which depend on the orbital occupation number $n_\alpha = n_{\alpha\uparrow} + n_{\alpha\downarrow}$. This eventually leads to the renormalized mean-field Hamiltonian

$$\begin{aligned} H_t^{\text{MF}} &= \sum_{ij\alpha\beta\sigma} g_t^{\alpha\beta} t_{ij}^{\alpha\beta} c_{i\alpha\sigma}^\dagger c_{j\beta\sigma}, \quad (6) \\ H_J^{\text{MF}, \chi/\Delta} &= \sum_r G_{J_r}^\alpha G_{J_r}^\beta H_{J_r}^{\chi/\Delta}, \end{aligned}$$

with $g_t^{\alpha\beta} = G_t^\alpha G_t^\beta$. One sees that, when $t_{ij}^{\alpha\beta} = t_{ij} \delta_{\alpha\beta}$, the above Hamiltonian reduces to the classical formulas of the single-band $t-J$ model for cuprate superconductors [40], where $g_t = G_t^2 = \frac{2p}{1+p}$, $g_J = G_J^2 = \frac{4}{(1+p)^2}$, with doping $p = 1 - n$. In the single-band system, the

physical superconducting order parameter is defined as $g_t|\Delta|$ [40]. In the multi-orbital system under consideration here, an immediate extension is made by employing the quantity $g_t^{\alpha\beta}|\Delta^{\alpha\beta}|$ to represent the $\alpha\beta$ -orbital component of the superconducting order parameter. It is worth noting that at zero temperature $T = 0$, approximate correspondence between the RMFT and $U(1)$ slave boson mean-field theory (SBMFT) [2, 52] self-consistent equations can be established if one assumes that $g_t^{\alpha\beta}$ is related to the Bose condensation of holons, and $\Delta^{\alpha\beta}$ is linked to the spinon pairing in SBMFT.

Fourier transforms to Eq. (4-6), we obtain the mean-field Hamiltonian in momentum space

$$H^{\text{MF}} = \sum_{\mathbf{k}} \Phi_{\mathbf{k}}^{\dagger} \begin{pmatrix} H_{t,\mathbf{k}}^{\text{MF}} + H_{J,\mathbf{k}}^{\text{MF},\chi} & H_{J,\mathbf{k}}^{\text{MF},\Delta} \\ [H_{J,\mathbf{k}}^{\text{MF},\Delta}]^{\dagger} & -[H_{t,\mathbf{k}}^{\text{MF}} + H_{J,\mathbf{k}}^{\text{MF},\chi}]^* \end{pmatrix} \Phi_{\mathbf{k}}, \quad (7)$$

where $\Phi_{\mathbf{k}} = (\Psi_{\mathbf{k}\uparrow}^T, \Psi_{-\mathbf{k}\downarrow}^{\dagger})^T$ is the corresponding Nambu basis set. This equation can be solved self-consistently, combining Eq. (2-3) to determine the final mean-field parameters, see also Supplementary Note 2 for more.

ACKNOWLEDGMENTS

The authors thank the helpful discussions with Xunwu Hu, Zhong-Yi Xie, and Guang-Ming Zhang. This project was supported by the National Key Research and Development Program of China (Grants No. 2022YFA1402802, 2018YFA0306001), the National Natural Science Foundation of China (Grants No. 92165204, No.12174454, No. 11974432, No.12274472), the Guangdong Basic and Applied Basic Research Foundation (Grants No. 2022A1515011618, No. 2021B1515120015), Guangdong Provincial Key Laboratory of Magnetoelectric Physics and Devices (Grant No. 2022B1212010008), Shenzhen International Quantum Academy (Grant No. SIQA202102), and Leading Talent Program of Guangdong Special Projects (201626003).

DATA AVAILABILITY

The data is available in https://github.com/ZhihuiLuo/RMFT_Ni327.

-
- [1] J. G. Bednorz and K. A. Müller, Possible high T_c superconductivity in the Ba-La-Cu-O system, *Z. Phys. B Condens. Matter* **64**, 189 (1986).
- [2] P. A. Lee, N. Nagaosa, and X.-G. Wen, Doping a mott insulator: Physics of high-temperature superconductivity, *Rev. Mod. Phys.* **78**, 17 (2006).
- [3] B. Keimer, S. A. Kivelson, M. R. Norman, S. Uchida, and J. Zaanen, From quantum matter to high-temperature superconductivity in copper oxides, *Nature* **518**, 179 (2015).
- [4] Z.-A. Ren et al., Superconductivity at 52 K in iron based F doped layered quaternary compound $\text{Pr}[\text{O}_{1-x}\text{F}_x]\text{FeAs}$, *Mater. Res. Innov.* **12**, 105 (2008).
- [5] X. Chen, T. Wu, G. Wu, R. Liu, H. Chen, and D. Fang, Superconductivity at 43 K in $\text{SmFeAsO}_{1-x}\text{F}_x$, *Nature* **453**, 761 (2008).
- [6] G. Chen et al., Superconductivity at 41 K and its competition with spin-density-wave instability in layered $\text{CeO}_{1-x}\text{F}_x\text{FeAs}$, *Phys. Rev. Lett.* **100**, 247002 (2008).
- [7] Z.-A. Ren et al., Superconductivity at 55 K in iron-based f-doped layered quaternary compound $\text{Sm}[\text{O}_{1-x}\text{F}_x]\text{FeAs}$, *Chinese Phys. Lett.* **453**, 2215 (2008).
- [8] J. Paglione and R. L. Greene, High-temperature superconductivity in iron-based materials, *Nat. Phys.* **6**, 645 (2010).
- [9] D. Li et al., Superconductivity in an infinite-layer nickelate, *Nature* **572**, 624 (2019).
- [10] D. Li et al., Superconducting dome in $\text{Nd}_{1-x}\text{Sr}_x\text{NiO}_2$ infinite layer films, *Phys. Rev. Lett.* **125**, 027001 (2020).
- [11] H. Sakakibara, H. Usui, K. Suzuki, T. Kotani, H. Aoki, and K. Kuroki, Model construction and a possibility of cupratelike pairing in a new d^9 nickelate superconductor $(\text{Nd}, \text{Sr})\text{NiO}_2$, *Phys. Rev. Lett.* **125**, 077003 (2020).
- [12] M. Kitatani, L. Si, O. Janson, R. Arita, Z. Zhong, and K. Held, Nickelate superconductors—a renaissance of the one-band hubbard model, *npj Quantum Mater.* **5**, 59 (2020).
- [13] F. Lechermann, Late transition metal oxides with infinite-layer structure: Nickelates versus cuprates, *Phys. Rev. B* **101**, 081110 (2020).
- [14] B. Kang et al., Infinite-layer nickelates as Ni- e_g Hund's metals, *npj Quantum Mater.* **8**, 35 (2023).
- [15] X. Wu et al., Robust $d_{x^2-y^2}$ -wave superconductivity of infinite-layer nickelates, *Phys. Rev. B* **101**, 060504 (2020).
- [16] Q. Gu et al., Single particle tunneling spectrum of superconducting $\text{Nd}_{1-x}\text{Sr}_x\text{NiO}_2$ thin films, *Nature communications* **11**, 6027 (2020).
- [17] H. Sun et al., Signatures of superconductivity near 80 K in a nickelate under high pressure, *Nature*, 1476 (2023).
- [18] J. Hou et al., Emergence of high-temperature superconducting phase in the pressurized $\text{La}_3\text{Ni}_2\text{O}_7$ crystals, *Chinese Phys. Lett.* **40**, 117302 (2023).
- [19] Y. Zhang et al., High-temperature superconductivity with zero-resistance and strange metal behavior in $\text{La}_3\text{Ni}_2\text{O}_{7-\delta}$, Preprint at arXiv:<https://arxiv.org/abs/2307.14819> (2024).
- [20] Z. Liu et al., Evidence for charge and spin density waves in single crystals of $\text{La}_3\text{Ni}_2\text{O}_7$ and $\text{La}_3\text{Ni}_2\text{O}_6$, *Sci. China Phys. Mech. Astron* **66**, 217411 (2023).
- [21] Z. Luo, X. Hu, M. Wang, W. Wú, and D.-X. Yao, Bilayer two-orbital model of $\text{La}_3\text{Ni}_2\text{O}_7$ under pressure, *Phys. Rev. Lett.* **131**, 126001 (2023).
- [22] F. Lechermann, J. Gondolf, S. Bötzel, and I. M. Eremin, Electronic correlations and superconducting instability in $\text{La}_3\text{Ni}_2\text{O}_7$ under high pressure, *Phys. Rev. B* **108**, L201121 (2023).

- [23] Y. Zhang, L.-F. Lin, A. Moreo, and E. Dagotto, Electronic structure, dimer physics, orbital-selective behavior, and magnetic tendencies in the bilayer nickelate superconductor $\text{La}_3\text{Ni}_2\text{O}_7$ under pressure, *Phys. Rev. B* **108**, L180510 (2023).
- [24] H. Sakakibara, N. Kitamine, M. Ochi, and K. Kuroki, Possible high T_c superconductivity in $\text{La}_3\text{Ni}_2\text{O}_7$ under high pressure through manifestation of a nearly half-filled bilayer hubbard model, *Phys. Rev. Lett.* **132**, 106002 (2024).
- [25] D. A. Shilenko and I. V. Leonov, Correlated electronic structure, orbital-selective behavior, and magnetic correlations in double-layer $\text{La}_3\text{Ni}_2\text{O}_7$ under pressure, *Phys. Rev. B* **108**, 125105 (2023).
- [26] R. Jiang, J. Hou, Z. Fan, Z.-J. Lang, and W. Ku, Pressure driven fractionalization of ionic spins results in cuprate-like high- T_c superconductivity in $\text{La}_3\text{Ni}_2\text{O}_7$, *Phys. Rev. Lett.* **132**, 126503 (2024).
- [27] B. Geisler, J. J. Hamlin, G. R. Stewart, R. G. Hennig, and P. Hirschfeld, Structural transitions, octahedral rotations, and electronic properties of $a_3\text{Ni}_2\text{O}_7$ rare-earth nickelates under high pressure, *npj Quantum Mater.* **9**, 38 (2024).
- [28] Z. Liu et al., Electronic correlations and partial gap in the bilayer nickelate $\text{La}_3\text{Ni}_2\text{O}_7$, Preprint at arXiv:https://arxiv.org/abs/2307.02950 (2024).
- [29] V. Pardo and W. E. Pickett, Metal-insulator transition in layered nickelates $\text{La}_3\text{Ni}_2\text{O}_{7-\delta}$ ($\delta = 0.0, 0.5, 1$), *Phys. Rev. B* **83**, 245128 (2011).
- [30] W. Wú, Z. Luo, D.-X. Yao, and M. Wang, Superexchange and charge transfer in the nickelate superconductor $\text{La}_3\text{Ni}_2\text{O}_7$ under pressure, *Sci. China Phys. Mech. Astron.* **67**, 117402 (2024).
- [31] Y.-f. Yang, G.-M. Zhang, and F.-C. Zhang, Interlayer valence bonds and two-component theory for high- T_c superconductivity of $\text{La}_3\text{Ni}_2\text{O}_7$ under pressure, *Phys. Rev. B* **108**, L201108 (2023).
- [32] V. Christiansson, F. Petocchi, and P. Werner, Correlated electronic structure of $\text{La}_3\text{Ni}_2\text{O}_7$ under pressure, *Phys. Rev. Lett.* **131**, 206501 (2023).
- [33] Q. Qin and Y.-f. Yang, High- T_c superconductivity by mobilizing local spin singlets and possible route to higher T_c in pressurized $\text{La}_3\text{Ni}_2\text{O}_7$, *Phys. Rev. B* **108**, L140504 (2023).
- [34] K. Jiang, Z. Wang, and F.-C. Zhang, High-temperature superconductivity in $\text{La}_3\text{Ni}_2\text{O}_7$, *Chinese Phys. Lett.* **41**, 017402 (2024).
- [35] Y. Shen, M. Qin, and G.-M. Zhang, Effective bilayer model Hamiltonian and density-matrix renormalization group study for the high- T_c superconductivity in $\text{La}_3\text{Ni}_2\text{O}_7$ under high pressure, *Chinese Phys. Lett.* **40**, 127401 (2023).
- [36] Q.-G. Yang, D. Wang, and Q.-H. Wang, Possible s_{\pm} -wave superconductivity in $\text{La}_3\text{Ni}_2\text{O}_7$, *Phys. Rev. B* **108**, L140505 (2023).
- [37] C. Lu, Z. Pan, F. Yang, and C. Wu, Interlayer-coupling-driven high-temperature superconductivity in $\text{La}_3\text{Ni}_2\text{O}_7$ under pressure, *Phys. Rev. Lett.* **132**, 146002 (2024).
- [38] X.-Z. Qu et al., Bilayer $t-J-J_{\perp}$ model and magnetically mediated pairing in the pressurized nickelate $\text{La}_3\text{Ni}_2\text{O}_7$, *Phys. Rev. Lett.* **132**, 036502 (2024).
- [39] Y.-B. Liu, J.-W. Mei, F. Ye, W.-Q. Chen, and F. Yang, s^{\pm} -wave pairing and the destructive role of apical-oxygen deficiencies in $\text{La}_3\text{Ni}_2\text{O}_7$ under pressure, *Phys. Rev. Lett.* **131**, 236002 (2023).
- [40] F. C. Zhang, C. Gros, T. M. Rice, and H. Shiba, A renormalised Hamiltonian approach to a resonant valence bond wavefunction, *Supercond. Sci. Technol.* **1**, 36 (1988).
- [41] P. W. Anderson, P. A. Lee, M. Randeria, T. M. Rice, N. Trivedi, and F. C. Zhang, The physics behind high-temperature superconducting cuprates: the ‘plain vanilla’ version of RVB, *J. Phys.: Condens. Matter* **16**, R755 (2004).
- [42] Q.-H. Wang, Z. D. Wang, Y. Chen, and F. C. Zhang, Unrestricted renormalized mean field theory of strongly correlated electron systems, *Phys. Rev. B* **73**, 092507 (2006).
- [43] P. W. Anderson, The resonating valence bond state in La_2CuO_4 and superconductivity, *Science* **235**, 1196 (1987).
- [44] Y. Gu, C. Le, Z. Yang, X. Wu, and J. Hu, Effective model and pairing tendency in bilayer Ni-based superconductor $\text{La}_3\text{Ni}_2\text{O}_7$, Preprint at arXiv:2306.07275 (2023).
- [45] Y. Zhang, L. F. Lin, A. Moreo, T. A. Maier, and E. Dagotto, Structural phase transition, s_{\pm} -wave pairing, and magnetic stripe order in bilayered superconductor $\text{La}_3\text{Ni}_2\text{O}_7$ under pressure, *Nat. Commun.* **15**, 2470 (2024).
- [46] Y.-H. Tian, Y. Chen, J.-M. Wang, R.-Q. He, and Z.-Y. Lu, Correlation effects and concomitant two-orbital s_{\pm} -wave superconductivity in $\text{La}_3\text{Ni}_2\text{O}_7$ under high pressure, *Phys. Rev. B* **109**, 165154 (2024).
- [47] W.-S. Wang, X.-M. He, D. Wang, Q.-H. Wang, Z. D. Wang, and F. C. Zhang, Finite-temperature gutzwiller projection for strongly correlated electron systems, *Phys. Rev. B* **82**, 125105 (2010).
- [48] J. Bünemann, W. Weber, and F. Gebhard, Multiband Gutzwiller wave functions for general on-site interactions, *Phys. Rev. B* **57**, 6896 (1998).
- [49] F. C. Zhang, Gossamer superconductor, mott insulator, and resonating valence bond state in correlated electron systems, *Phys. Rev. Lett.* **90**, 207002 (2003).
- [50] J. Y. Gan, Y. Chen, Z. B. Su, and F. C. Zhang, Gossamer superconductivity near antiferromagnetic mott insulator in layered organic conductors, *Phys. Rev. Lett.* **94**, 067005 (2005).
- [51] B. Edegger, V. N. Muthukumar, and C. Gros, Gutzwiller–RVB theory of high-temperature superconductivity: Results from renormalized mean-field theory and variational monte carlo calculations, *Adv. Phys.* **56**, 927 (2007).
- [52] G. Kotliar and J. Liu, Superexchange mechanism and d-wave superconductivity, *Phys. Rev. B* **38**, 5142 (1988).

AUTHOR CONTRIBUTIONS

Z.L. and B.L. contributed equally. D.X.Y. and W.W. conceived and designed the project. Z. L. wrote the code. Z.L. and B.L. performed the theoretical calculations and corresponding analysis under the supervision of D.X.Y. and W.W. All authors contributed to the interpretation of the results and wrote the paper.

COMPETING INTERESTS

The authors declare no competing interests.